applied sciences

MDPI

Article

Study on Preparation and Processing Properties of Mechano-Chemical Micro-Grinding Tools

Xin Song [1,2], Feifan Ke [1], Keyi Zhu [1,*], Yinghui Ren [1], Jiaheng Zhou [1] and Wei Li [1]

[1] College of Mechanical and Vehicle Engineering, Hunan University, Changsha 410082, China; feifanke@hnu.edu.cn (F.K.); rebecca_ryh@163.com (Y.R.); zjheng1997@163.com (J.Z.); liwei@hnu.edu.cn (W.L.)
[2] CSSC Intelligent Technology Shanghai Co., Ltd., Shanghai 200011, China; songxin716@126.com
* Correspondence: keyizhu@hnu.edu.cn

Abstract: The application of hard and brittle materials such as single-crystal silicon in small parts has expanded sharply, and the requirements for their dimensional accuracy and processing surface quality have been continuously improved. This paper proposes using mechano-chemical micro-grinding tools to process single-crystal silicon, which can realize the high-quality and efficient processing of such tiny parts through mechano-chemical composite action. The microstructure composition of the mechano-chemical micro-grinding tools was designed, the theoretical analysis model of grinding force was established and verified by experiments, and the temperature field distribution during mechano-chemical micro-grinding of single-crystal silicon was simulated and studied, which provided a theoretical basis for mechano-chemical action. Special micro-grinding tools were developed, and mechano-chemical micro-grinding processing tests were carried out. The results show that the coupling synergy of grinding force and grinding temperature improves the chemical activity of the micro-grinding tools, thereby promoting the solid–solid phase chemical reaction of abrasives and additives at the sharp points of the surface of the micro-grinding tools. And when the content of cerium oxide abrasive is 25%, it is more conducive to the solid–solid phase chemical reaction, and calcium oxide can be used as an additive to promote the active agent of solid–solid phase chemical reaction, improve the degree of chemical reaction, and thus improve the removal rate of materials. Soft reactants that are easy to remove are generated on the surface of monocrystalline silicon and are removed by the mechanical friction between the abrasive grain and the surface of the silicon wafer, and finally achieve low-damage processing with a surface roughness of Ra1.332 nm, which is much better than the surface roughness of Ra96.363 nm after diamond abrasive processing.

Keywords: mechano-chemical; micro-grinding tools; micro-grinding; grinding performance; grinding force

Citation: Song, X.; Ke, F.; Zhu, K.; Ren, Y.; Zhou, J.; Li, W. Study on Preparation and Processing Properties of Mechano-Chemical Micro-Grinding Tools. *Appl. Sci.* **2023**, *13*, 6599. https://doi.org/10.3390/app13116599

Academic Editor: Mark J. Jackson

Received: 5 May 2023
Revised: 24 May 2023
Accepted: 26 May 2023
Published: 29 May 2023

1. Introduction

The application of small parts of hard and brittle materials such as single-crystal silicon is increasingly extensive, such as the manufacture of complex surface structure silicon microchannel plates, aspheric microlens molds, and other devices. However, such parts are usually processed with small feature sizes, and the surface quality and dimensional accuracy requirements are very high, usually requiring the surface of the silicon wafer to achieve nanometer roughness while also requiring no damage to the subsurface [1–4]. Although the current micro-grinding technology can process silicon-based small and complex structural parts, it easily produces cracks, chipping, missing corners, and other damage [5–7]. Therefore, conducting in-depth research on the efficient and high-precision machining of small parts of complex structures is necessary.

Mechano-chemical grinding (MCG) technology is an ultra-precision machining method that couples mechanical action and chemical reaction, which was first proposed by the team of Zhou Libo of Ibaraki University in Japan [8]. With the proper grinding parameters, MCG technology can produce ultra-high quality surfaces with a surface roughness of Ra < 1 nm [9,10], and its ground surface quality is comparable to chemical-mechanical polishing (CMP) technology. Zhou et al. [11–13] observed silicon wafers processed by mechanochemical grinding with TEM and found no subsurface damage, proving that MCG can achieve subsurface damage processing under suitable parameters. Wu et al. [14] believed that MCG was a chemical and mechanical interaction process, and only when the two interactions reached a certain equilibrium could a surface without subsurface damage be obtained. When the mechanical action was stronger than the chemical action, a subsurface damage layer of a certain thickness would be produced. Tian et al. [15] used grinding wheels to process silicon wafers with MCG technology, observed the change process of grinding surface morphology and the material removal mechanism of MCG processing, and studied the relationship between material removal rate and surface roughness. The results showed that the MCG process could eliminate the scratches caused by the ordinary grinding process, and the material removal rate decreases with surface roughness. Additionally, MCG technology can eliminate surface defects such as scratches left by diamond grinding wheels on the surface of the workpiece in the previous process. Therefore, it is possible to use diamond grinding wheels for efficient machining with a large margin, and then high-quality machining with MCG to obtain a high-precision surface.

Although MCG technology can solve the problems of large edge damage and poor surface quality in the processing of small parts, it is mainly used for the backside thinning processing of large-size silicon wafers, and most of the existing research is to analyze the removal mechanism of MCG. It needs more research on micro-grinding tools for mechano-chemical micro-grinding. Therefore, according to the principle of mechano-chemical grinding and the material characteristics of single-crystal silicon, this paper designed and developed mechano-chemical micro-grinding tools, established a theoretical analysis model of grinding force and verified it by experiment, and studied the processing technology and grinding performance of mechano-chemical micro-grinding tools, which made up for the shortcomings of existing research in the field of micro-grinding.

2. Design of Mechano-Chemical Micro-Grinding Tools

Unlike traditional grinding processing, which uses an abrasive higher than the hardness of the material to be processed to remove the brittleness or plasticity of single-crystal silicon, mechanochemical grinding achieves material removal through the solid–solid phase chemical reaction between the abrasive and additives and the surface of the material, as well as the synergistic effect of mechanical stress [16]. Therefore, the design of micro-grinding tools usually needs to meet four conditions:

(1) The hardness of the abrasive is lower than that of the material being processed;
(2) The abrasive can undergo a solid–solid phase chemical reaction with the processed material;
(3) Abrasive additives can directly react with the material to be processed or can promote solid–solid phase chemical reactions;
(4) Abrasive additives can adjust the porosity ratio of the abrasive.

Based on the above conditions, this paper made a reasonable selection of the microstructure components of the abrasive in three aspects: abrasives, binders, and additives, and reflected the microstructure of the abrasives through the content ratio. Cerium oxide was selected as an abrasive, which has a lower hardness than single-crystal silicon, has an excellent grinding effect, and is not easy to clog [17]. The phenolic resin was selected as the binder. The micro-grinding tools made of it usually have good elasticity and self-sharpening, and it is easy to obtain a good processing surface. Sodium bicarbonate, zinc sulfate, calcium oxide, and copper powder were selected as additives, which can enhance the chemical activity of the abrasive, thereby improving the grinding performance of mechano-chemical micro-grinding tools to achieve the purpose of high-quality processing [18]. The main functions of each component of the additive are as follows.

(1) Sodium bicarbonate: Sodium bicarbonate will decompose under hot pressing conditions of about 190 °C to produce carbon dioxide gas and sodium carbonate. Carbon

dioxide gas can make certain pores in the micro-grinding tools, thereby ensuring the self-sharpening of the micro-grinding tools. The sodium carbonate produced by decomposition can be used as an active agent to weaken the adhesion between the cerium oxide abrasive and the binder, thereby enhancing the self-sharpening of the micro-grinding tools;

(2) Zinc sulfate: Adding zinc sulfate to the abrasive can make the additive particles adsorb around the abrasive. After the abrasive particles adsorb the particles, they are more likely to be broken in the mechanical collision during grinding, thereby increasing the specific surface area of the abrasive particles and improving the chemical activity;

(3) Calcium oxide: Calcium oxide acts as a curing agent in additives and can promote the curing of the resin. Furthermore, because of its good heat resistance and high bonding strength, it can play a hygroscopic role in micro-grinding tools;

(4) Copper powder: Because copper powder has good thermal conductivity, the heat generated by the interaction between the abrasive and the workpiece during the grinding process can be conducted through the copper powder, improving the overall heat resistance of the micro-grinding tools.

The design size of the individual micro-grinding tool is 10 mm in diameter and 8 mm in height, and the composition ratio is shown in Table 1.

Table 1. The composition ratio of micro-grinding tools (*vol*%).

Cerium Oxide	Phenolic Resin	Sodium Bicarbonate	Zinc Sulfate	Calcium Oxide	Copper Powder
25	15	20	10	5	5

After calculating the amount of each ingredient added, follow these steps to make a micro-abrasive:

(1) Screening: After grinding the powder, use the #400 screen for screening, filter out larger particles, and improve the uniformity of the powder, so that the components can be mixed more evenly;

(2) Weighing: To prevent the loss of raw materials in the subsequent baking and mixing process, 120% of the theoretical feeding amount calculated by each component should be weighed after the screening;

(3) Drying: To prevent the powder's moisture from affecting the abrasive's performance, the weighed powder should be dried. In this experiment, each powder was placed in an electric constant temperature drying oven and kept warm at 50 °C for 30 min.

(4) Mixing powder: The ingredients are mixed according to the different proportions of the design, and the ingredients are evenly mixed by stirring;

(5) Hot pressing of filler: The abovementioned evenly mixed powder is filled into the mold sprayed with mold release agent according to the total theoretical mass and placed under the hot press machine for hot pressing operation. The hot pressing conditions are pressure 5 MPa, temperature 180 °C, and holding time of 40 min;

(6) Secondary curing: After the preliminary hot pressing operation, the cylindrical micro-grinding tool has a certain hardness and strength but is not fully cured. The electric constant temperature drying oven is used to carry out the secondary curing operation of the micro-grinding tool. At the same time, to make the micro-grinding tool heat evenly, it needs to be buried in quartz sand for heating;

(7) Preservation of micro-grinding tools: The micro-grinding tools made after the above steps are kept in a sealed bag after they are lowered to room temperature. The overall preparation process of the micro-grinding tools is shown in Figure 1.

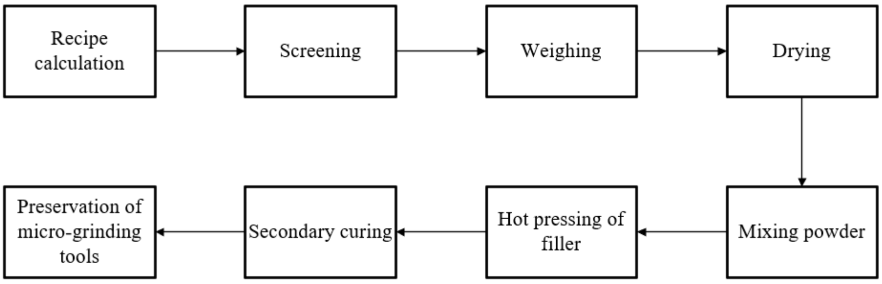

Figure 1. Preparation flow chart of micro-grinding tools.

Using the MKC2945C continuous trajectory coordinate grinding machine as the processing platform, the cylindrical mechanochemical micro-grinding tool shown in Figure 2 was ground and processed experimentally. The micro-grinding tool was fixed on the fixture, and the micro-grinding tool was driven by the rotation of the electric spindle of the machine tool, and then the single-crystal silicon was ground. The processing site is shown in Figure 3.

Figure 2. The physical object of micro-grinding tools.

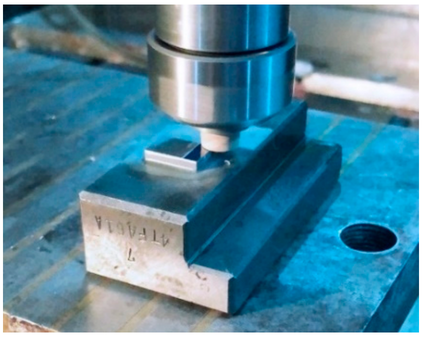

Figure 3. The grinding of the micro-grinding tool.

3. Analysis of Micro-Grinding Force

3.1. Theoretical Analysis of Grinding Force

Since the soft layer generated by the reaction will undergo a certain degree of elastoplastic deformation under the normal force of the micro-grinding tool, a coefficient ε of the contact geometry deformation of the reaction abrasive and silicon wafer is introduced in this paper, and the grinding force formula can be expressed as

$$\vec{F} = \vec{F_n} + \vec{F_t} \tag{1}$$

$$F_n = \varepsilon\left(F_{nf} + F_{nc}\right) \tag{2}$$

$$F_t = \varepsilon\left(F_{tf} + F_{tc}\right) \tag{3}$$

where F_n is the normal grinding force of the abrasive grain, F_t is the tangential grinding force of the abrasive grain, F_{nf} is the normal friction force, F_{nc} is the normal cutting force, F_{tf} is the tangential friction force, and F_{tc} is the tangential cutting force.

Figure 4 is a schematic diagram of the force on the abrasive grain.

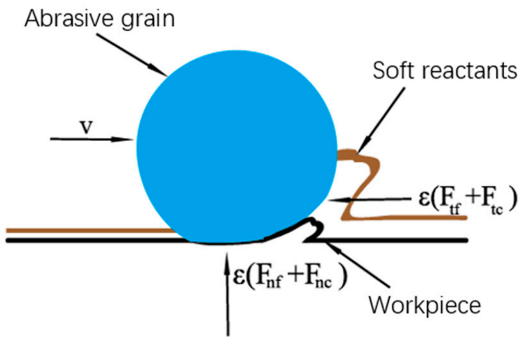

Figure 4. Schematic diagram of abrasive grain stress.

3.1.1. Grinding Depth Model of the Abrasive

When the micro-grinding tool processes, the scratches on the surface of the workpiece can reflect the motion state of the abrasive, and the volume of the removed single-crystal silicon can be expressed by the product of the length of the abrasive mark and the average cutting area of the abrasive. When grinding, the silicon wafer is in a stationary state, and the grinding width is the radius of the soft abrasive, that is, the center of the abrasive disc moves on the edge of the silicon wafer. To obtain the length of the wear mark, the coordinate system shown in Figure 5 is established with O point as the origin of the coordinate system, OD on the geometric center line of the silicon wafer, O' as the geometric center of the micro-grinding tool, and the apex A in the contact zone between the micro-grinding tool and the silicon wafer is assumed to be l away from AO, and let l be the variable.

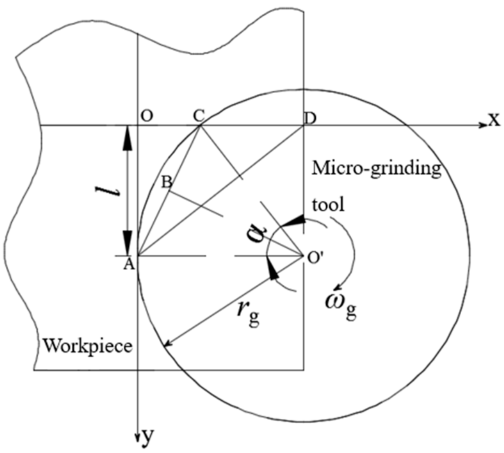

Figure 5. Schematic diagram of material removal.

The geometric relationship can be deduced from the relationship between the rotation angle of the micro-grinding tool α and l, as shown in Equation (4).

$$\alpha = arccos\sqrt{1-\left(\frac{l}{r_g}\right)^2} \tag{4}$$

where r_g is the radius of the micro-grinding tool, and l is the distance between the contact area's vertex and the silicon wafer's centerline.

The abrasive mark length $L(l)$ can be expressed as the product of the micro-grinding tool's angle and the micro-grinding tool's radius, as shown in Equation (5).

$$L(l) = r_g \cdot \alpha = r_g \cdot arccos\sqrt{1-\left(\frac{l}{R_g}\right)^2} \tag{5}$$

The instantaneous amount of material removed dV from the geometric centerline l of the silicon wafer is shown in Equation (6).

$$dV = S \cdot L(l) \cdot \beta \cdot N \tag{6}$$

where *L(l)* is the length of the wear mark at the geometric centerline l of the silicon wafer, S is the material removal area of a single abrasive grain, β is the repetitive cutting coefficient of the abrasive grain, and the value is 0.66 [19]; N is the number of effective abrasive grains from the center of the end face geometry of the micro-grinding tool.

The instantaneous removal volume of the material can be calculated as shown in Equation (7).

$$dV = r_g \cdot \gamma \cdot \left[\frac{2(r_a - z_g)}{r_a}\right]^{2.5} \cdot \left(1 - \frac{l^2}{r_g^2}\right)^{-0.5} \cdot \beta dl \tag{7}$$

Among them, γ is the volume ratio of the abrasive, and $r_a - z_g$ is the maximum grinding depth of the abrasive.

The average depth of cut can be further calculated as shown in Equation (8).

$$d_a = \frac{1}{2}(r_a - z_g) = \frac{r_a}{4}\left(\frac{2\pi \cdot l \cdot a_p}{\omega_g r_g \cdot \beta \cdot \gamma}\sqrt{1 - \frac{l^2}{r_g^2}}\right)^{0.4} \tag{8}$$

where ω_g is the speed of the abrasive, and a_p is the depth of cut for a given micro-grinding tool.

As can be seen from the results of Equation (8), factors such as the size of the micro-grinding tool and the size of the abrasive grain will impact the material removal volume of the micro-grinding tool. It can also be seen that even under the condition of a macroscopic depth of cut, a change in the grinding position causes a change in the depth of the cut.

3.1.2. The Friction and Cutting Force of a Single Abrasive Grain

The micro-grinding tool is in mechanical contact with the surface of the silicon wafer by mechanical action during the grinding process. The normal force caused by friction can be expressed as a function of the depth of cut of the abrasive [20], as shown in Equation (9).

$$F_{nf} = \sqrt{\frac{16\mathrm{d}_a^3 \cdot r_a \cdot E^{*2}}{9}} \tag{9}$$

where E^* is the equivalent modulus of elasticity.

It can be further calculated to obtain

$$F_{nf} = \frac{r_a^2}{6\left((1 - v_1^2)/\eta E_1 + (1 - v_2^2)/E_2\right)}\left(\frac{2\pi \cdot l \cdot a_p}{\omega_g r_g \cdot \beta \cdot \gamma}\sqrt{1 - \frac{l^2}{r_g^2}}\right)^{0.6} \tag{10}$$

where E_1 and E_2 are the elastic moduli of single-crystal silicon and cerium oxide, respectively, and v_1 and v_2 are Poisson's ratios of monocrystalline silicon and cerium oxide abrasives, respectively.

The tangential force caused by friction can be obtained by multiplying the normal force by μ friction coefficient (the friction coefficient between the micro-grinding tool and the silicon wafer at room temperature μ = 0.327).

For the grinding force model of a single abrasive grain, the normal grinding force is formed during the grinding process due to the generation of chips, which is proportional to the corresponding cross-sectional area. It is obtained by calculation that

$$F_{nc} = \frac{4r_a^2 \cdot k}{15}\left(\frac{2\pi \cdot l \cdot a_p}{\omega_g r_g \cdot \beta \cdot \gamma}\sqrt{1 - \frac{l^2}{r_g^2}}\right)^{0.6} \tag{11}$$

where k is the chip thickness coefficient, which is related to the properties of the material being processed.

When chips are generated during the grinding process, the resulting normal and tangential forces are proportional [21]. For (100) crystal-oriented single-crystal silicon, the scale factor $\delta = 0.58$. Combined with the self-introduced geometric deformation coefficient, the expression of the total normal grinding force and tangential grinding force during the grinding is shown in Equations (12) and (13).

$$F_n = \varepsilon\left(F_{nf} + F_{nc}\right) = \varepsilon\left[\frac{r_a^2}{6\left(\frac{1-v_1^2}{\eta E_1} + \frac{1-v_2^2}{E_2}\right)} + \frac{4r_a^2 \cdot k}{15}\right] \cdot \left(\frac{2\pi \cdot l \cdot a_p}{\omega_g r_g \cdot \beta \cdot \gamma}\sqrt{1 - \frac{l^2}{r_g^2}}\right)^{0.6} \tag{12}$$

$$F_t = \varepsilon\left(F_{tf} + F_{tc}\right) = \varepsilon\left[\frac{\mu r_a^2}{6\left(\frac{1-v_1^2}{\eta E_1} + \frac{1-v_2^2}{E_2}\right)} + \frac{4r_a^2 \cdot k \cdot \delta}{15}\right] \cdot \left(\frac{2\pi \cdot l \cdot a_p}{\omega_g r_g \cdot \beta \cdot \gamma}\sqrt{1 - \frac{l^2}{r_g^2}}\right)^{0.6} \tag{13}$$

It can be seen from Equations (12) and (13) that the characteristics of the micro-grinding tool itself, including changes in the abrasive diameter, modulus of elasticity, abrasive volume ratio, and other factors, will affect the grinding force. At the same time, changes in grinding parameters such as speed and cutting depth will also affect the change in grinding force.

3.2. Experimental Study of Grinding Force

To verify the model's accuracy, the grinding force of the surface of the silicon wafer ground by the micro-grinding tool was measured experimentally. The experiment was performed on the MKC2945C continuous trajectory coordinate grinder. The experimental silicon wafer is commercially purchased (100) crystalline single-crystal silicon with a size of 15 × 10 × 3 mm; The sensor is a KISTLER load cell. In this experiment, the end-face grinding method is adopted, and Figure 6 is the diagram of the experimental device.

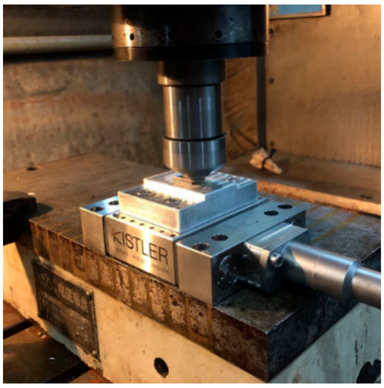

Figure 6. Device diagram of the grinding force experiment.

In the experiment, the fixture of the silicon wafer was first designed and fixed to the sensor with a countersunk bolt, and the silicon wafer was fixed on the fixture for the grinding force test. The grinding force on the silicon wafer is transmitted to the sensor through the fixture, resulting in force signal data in three spatial coordinate directions. After the tool was set between the tool and the workpiece, a single 1 μm axial feed was carried out, followed by a reciprocating lateral feed, and the above process was repeated to complete the grinding process. The processing parameters are shown in Table 2.

Table 2. Processing parameters of the grinding experiment.

Project	Parameter
Speed (r/min)	1500
Axial feed speed (μm/min)	1
Processing time (h)	1
No feed light grinding times	10
Transverse feed speed (mm/min)	10
Grinding method	Dry grinding

After the grinding state was stable, the data was collected. Figure 7 shows the normal and tangential grinding forces under different cutting depth conditions after filtering treatment, and the sensor data acquisition time is 10 s. The variable for this grinding force measurement experiment is the depth of cutting.

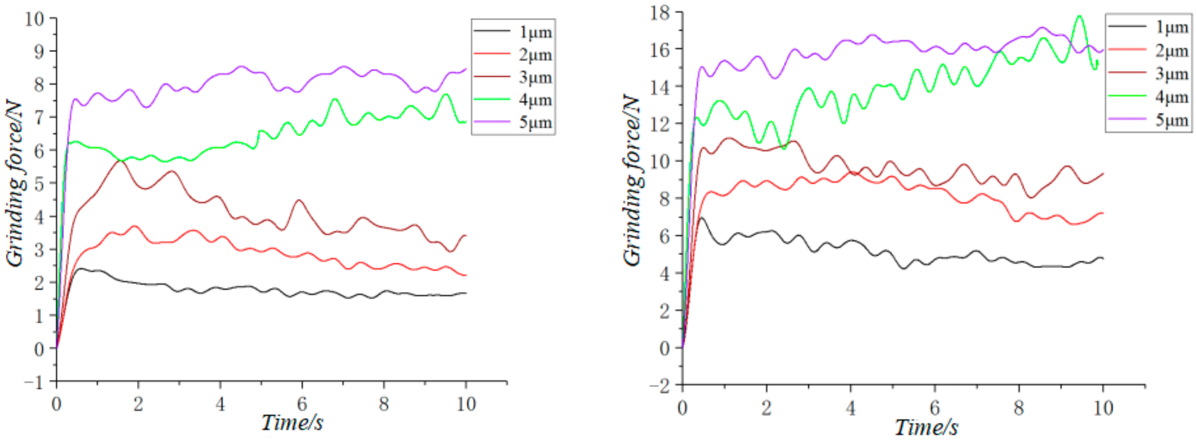

(**a**) (**b**)

Figure 7. The grinding force under different depths of cut conditions. (**a**) Tangential grinding force. (**b**) Normal grinding force.

From the grinding force measurement results in Figure 7, it can be seen that after filtering, both the normal grinding force and the tangential grinding force will show fluctuations within a certain range. The cause of this phenomenon may be fluctuations in force caused by the system's vibration. In addition, from the grinding force measurement results of Figure 7a,b, it can be seen that when the grinding depth is 1~3 μm, the grinding force will decrease to a certain extent as the grinding process progresses. Illustrating that at a given cutting depth, material removal occurs at the contact surface of the micro-grinding tool and silicon wafer, decreasing the contact pressure between the two contact surfaces. When the cutting depth is 4~5 μm, the grinding force does not show a decreasing trend, which may be due to the average particle size of cerium oxide abrasive grain being 5 μm; when the cutting depth reaches 4~5 μm, it has exceeded the cutting edge height of cerium oxide abrasive grain. At this time, the deformation degree of the abrasive grain is large, and there is a more serious extrusion phenomenon between the micro-grinding tool and the silicon wafer, so the measured grinding force is large.

To reflect the grinding force more realistically, the average data points within 0.5~4 s after the rising stage of each force measurement result were compared, and the results after adjusting the selected interval are shown in Figure 8.

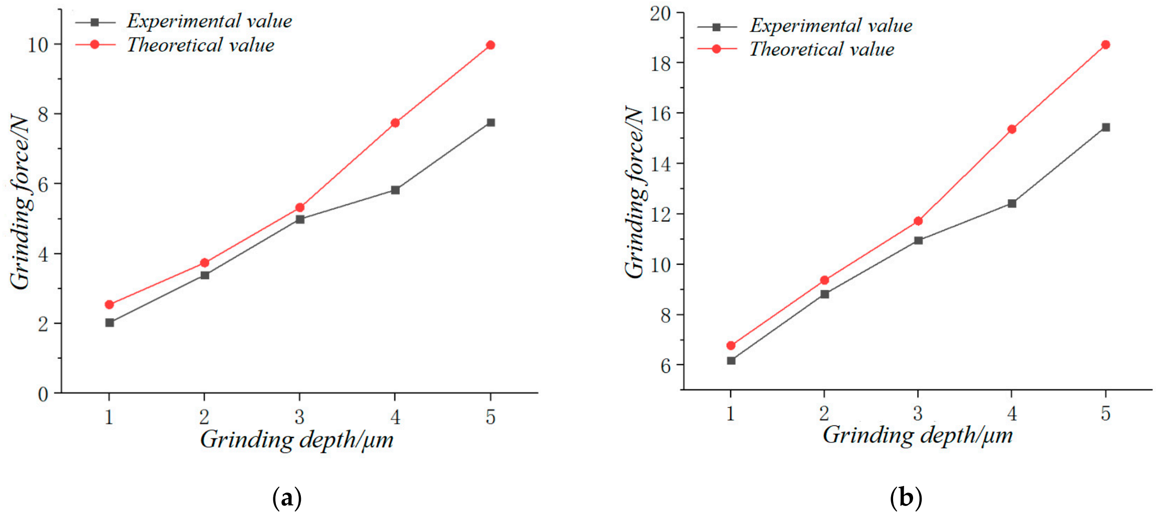

Figure 8. Comparison of experimental and theoretical grinding force values in the initial stage. (**a**) Tangential grinding force. (**b**) Normal grinding force.

It can be seen from the results of Figure 8 that after changing the sampling time range of the grinding force, the experimental value and theoretical value of the grinding force at a cutting depth of 1~3 μm were greatly reduced, both of which were about 10%. In contrast, the error at a cutting depth of 4~5 μm increased. This phenomenon may be because the average particle size of the abrasive grain used was 5 μm. Its hardness is close to the hardness of the processed single-crystal silicon, and the cutting depth of 4~5 μm exceeded the cutting edge height of the abrasive grain.

From the above-shown results, it can be seen that the prediction error of normal grinding force is small in terms of the error between the theoretical and experimental values of the model. Without changing the size of the micro-grinding tool and silicon wafer, the change of the speed and axial feed speed will affect the grinding force, and the grinding force increases with the increase of the feed speed and decreases with the increase of the speed.

4. Simulation Analysis of Grinding Temperature

To study the temperature distribution of silicon materials processed by mechano-chemical micro-grinding tools, ABAQUS software (https://en.wikipedia.org/wiki/Abaqus#External_links) was used for finite element simulation analysis. When analyzing the grinding temperature, since both contact surfaces satisfy the heat transfer equation, the study object can be discretized to study the tiny cells.

4.1. Material Parameters and Model Building

The material property parameters required for triboscopic heat generation and heat transfer analysis are density, Poisson's ratio, Young's modulus, coefficient of thermal expansion, thermal conductivity, and specific heat. The material property parameters are shown in Table 3.

Table 3. Properties of materials.

Material	Density g/cm^3	Young's Modulus GPa	Poisson's Ratio	Coefficient of Thermal Expansion K^{-1}	Thermal Conductivity $W\cdot(m\cdot K)^{-1}$	Specific Heat $J\cdot(kg\cdot K)^{-1}$
Single-crystal silicon	2.329	131	0.28	2.6×10^{-6}	150	700
Cerium dioxide	7.132	165	0.5	10×10^{-6}	20	359

For the micro-grinding tools and silicon wafers, the areas affected by mechano-chemical grinding are all thin layers of contact surfaces, so to reduce the number of invalid calculations, the model is simplified to 1 mm for both the abrasive and silicon wafers, and the size of the silicon wafers is reduced appropriately to 3 mm $\times$ 3 mm, and the part module of the software is used for modeling.

Define material properties and test boundary conditions, and mesh the model via the software's Mesh module. Since only the temperature is analyzed in this paper, and the geometry of the abrasive and the processed silicon wafer is regular, the hexahedral mesh and C3D8T cell type, three-way linear displacement, and three-way linear temperature are selected. Figure 9 shows the result of meshing, where the simplified abrasive contains 30,317 grid elements, and the simplified silicon wafer contains 6250 mesh elements.

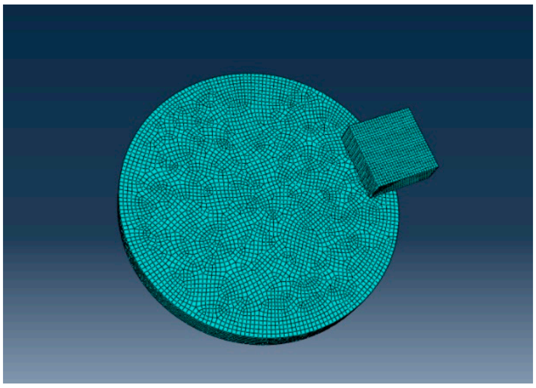

Figure 9. Simplified finite element model of micro-grinding tool and silicon wafer.

4.2. Temperature Distribution Characteristics

The grinding temperature comes from the mutual friction between the two contact surfaces. Due to the fast friction speed, the temperature rise rate is higher than the heat loss rate caused by the heat conduction of the silicon wafer and the micro-grinding tool itself. Figure 10 shows the temperature distribution of the abrasive surface, and the grinding time is 1 s, 2 s, 3 s, and 5 s, respectively. As can be seen from Figure 10, the maximum temperature of the contact point between the silicon wafer and the abrasive is 57.4 °C, 70.5 °C, 88.0 °C, and 144 °C. The simulation results show that as the grinding time increases, the temperature generated by the contact surface of the abrasive and the silicon wafer also increases. Moreover, it can also be seen from Figure 10 that the heat source is mainly concentrated on the edge of the abrasive, which is mainly due to the high linear velocity at the edge of the abrasive and the longer friction distance at the same time. As a result, the temperature at the edge of the abrasive is higher than in the internal area, and material removal is more likely to occur.

Due to the low hardness and small particles of the abrasives and additives, they are prone to crushing and heat generation during grinding. The instantaneous maximum heat generated by the powder crushing caused by friction between the two contact surfaces can be calculated by Equation (14).

$$Q = \frac{0.236\mu WV}{l\left[K_A + 0.88K_B\left(\frac{Vl}{K_B}\right)^{0.5}\right]} \tag{14}$$

where μ is the sliding friction coefficient, W is the vertical weight of the contact point, V is the sliding speed, l is the perimeter of the contact area, and K_A and K_B are the thermal conductivity of the two contact objects.

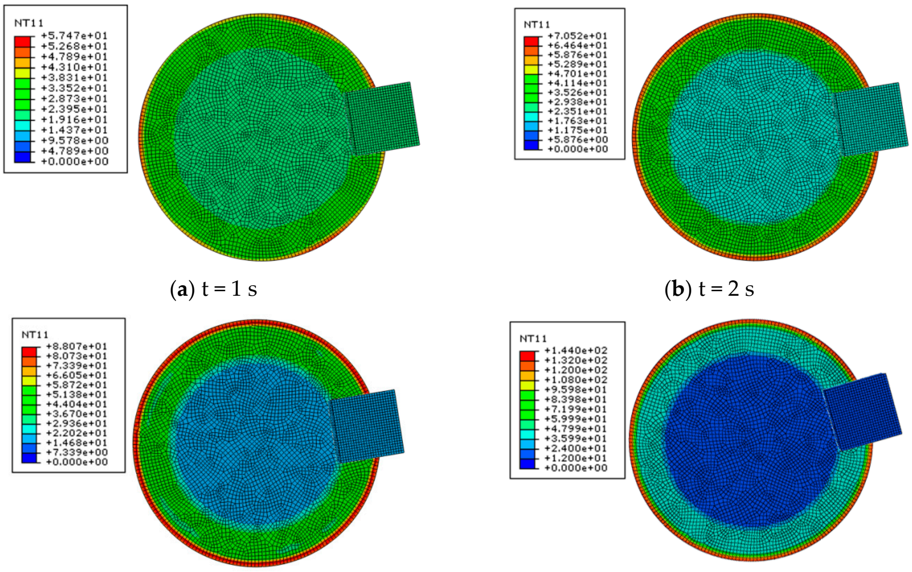

(**a**) t = 1 s (**b**) t = 2 s

(**c**) t = 3 s (**d**) t = 5 s

Figure 10. Simulated temperature distribution cloud.

Substituting the relevant data into the calculation Equation (14) shows that a high temperature of more than 1000 *K* can be generated during grinding, and the temperature threshold for solid phase reaction between cerium oxide and single-crystal silicon can be reached [16]. Therefore, based on the above analysis, it can be preliminarily concluded that under the test conditions in this paper, the self-made micro-grinding tools can undergo solid–solid phase chemical reactions when grinding silicon wafers.

5. Performance Analysis of the Micro-Grinding Tools

5.1. Microscopic Topography

Scanning electron microscopy (SEM) was used to observe the end topography of the micro-grinding tool, as shown in Figure 11. Because the micro-grinding tool is made by hot pressing at higher pressure, the overall compactness of the structure is high, and the abrasive grain distribution is uniform. Since sodium bicarbonate is decomposed by heat to produce gas, there are pores in the matrix of the micro-grinding tool for chip removal and heat dissipation.

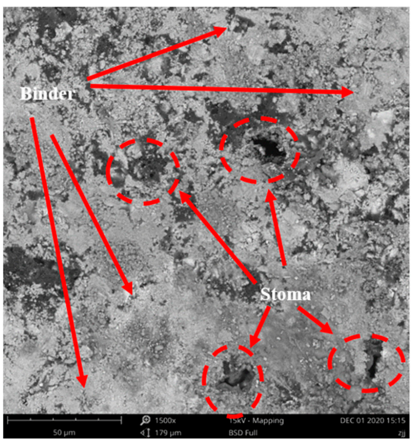

Figure 11. Surface micromorphology of the micro-grinding tool.

5.2. Micro-Grinding Performance

5.2.1. Experimental Conditions

The experimental conditions for the grinding performance of mechano-chemical micro-grinding tools are the same as those for grinding force measurement. After grinding, a white light interferometer (ZYGO New View 7100) is used to measure the surface roughness after grinding.

The silicon wafer processed by mechano-chemical micro-grinding tools and diamond grinding tools is shown in Figure 12, the left side is the silicon wafer processed by mechano-chemical micro-grinding tools, and the right side is the silicon wafer processed by diamond grinding tools. It can be seen that the self-made micro-grinding tool can grind the single-crystal silicon into a smooth surface with a specular reflection effect. The surface of the diamond grinding tool with the same mesh number is relatively rough under the same process conditions, does not show mirror luster, and there are obvious scratches.

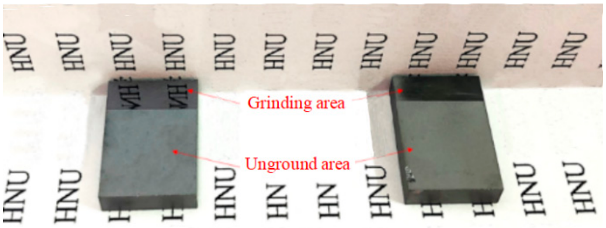

Figure 12. Actual view of the silicon wafer after processing.

5.2.2. Results and Discussion

In this experiment, the self-made micro-grinding tools, diamond grinding tools of the same mesh and size, and commercially purchased silicon wafers processed by CMP were compared under the same process conditions, and the surface morphology was observed. Figure 13 shows the micromorphology comparison of the grinding area and the unground area of the silicon wafer processed under the ultra-depth microscope. It can be seen that the self-made micro-grinding tool can process the originally rough surface of the single-crystal silicon very smoothly. Figure 14 shows the surface topography of a silicon wafer ultra-depth of field microscope after using a diamond grinding tool, a self-made micro-grinding tool, and CMP processing. From the observation of Figure 14, it can be seen that the surface of the silicon wafer after diamond grinding tool processing shows very obvious processing traces and processing defects such as crushing and pits. The surface of the silicon wafer processed by self-made micro-grinding tools and CMP has no obvious processing scratches and no processing defects such as crushing, scratches, and pits.

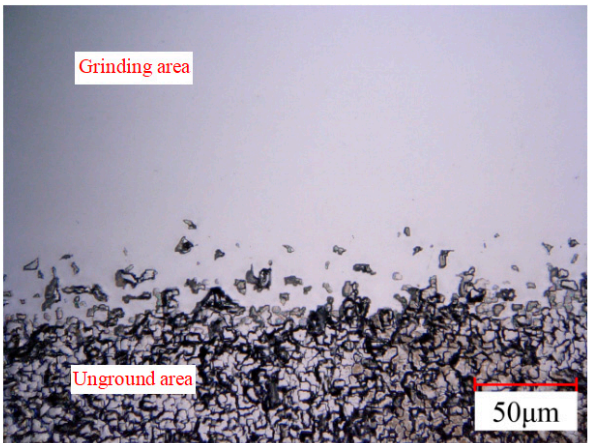

Figure 13. Micromorphology of single-crystal silicon grinding zone and unground area.

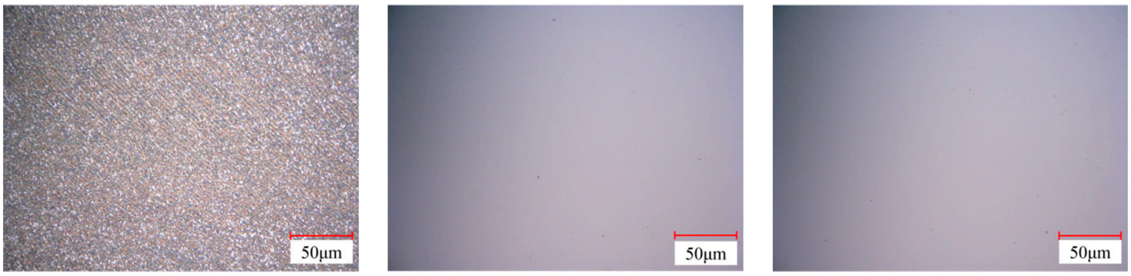

(a) (b) (c)

Figure 14. Micromorphology of silicon wafer processed by different processing methods. (**a**) Diamond grinding tools processing. (**b**) Self-made micro-grinding tools processing. (**c**) CMP processing.

The measurement results of surface roughness are shown in Figure 15. The measurement results showed that the surface of the silicon wafer, after the processing of self-made micro-grinding tools and diamond grinding tools, had a recognizable directional grinding texture. The measurement results showed that the surface roughness of silicon wafers after grinding self-made micro-grinding tools was Ra = 1.332 nm. In contrast, the surface roughness of silicon wafers after grinding diamond grinding tools was Ra = 96.363 nm, and the grinding effect of self-made micro-grinding tools was much better than that of diamond grinding tools. Analyzing the above phenomenon, it was found that the self-made micro-grinding tool was a soft reaction layer through the chemical reaction between the abrasive and the surface material of the silicon wafer. Then, the surface material was removed through the mechanical action between the abrasive and the silicon wafer to form an ultra-smooth and ultra-low damage silicon wafer surface.

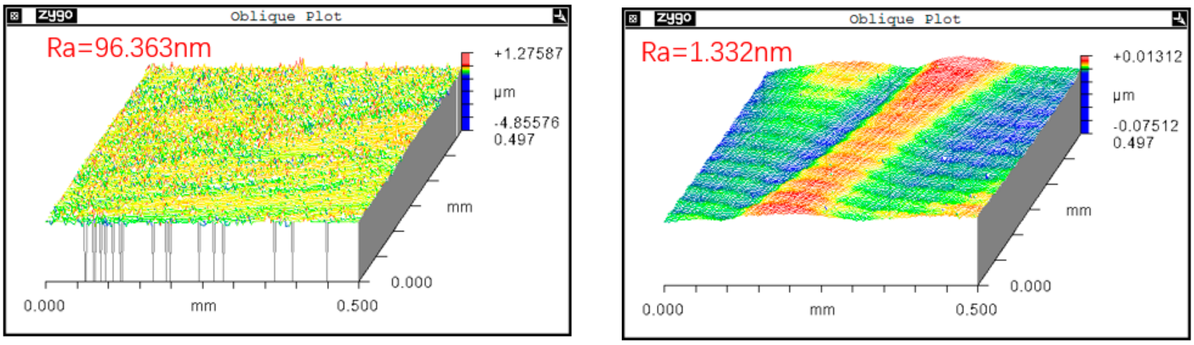

(a) (b)

Figure 15. Results of measuring surface roughness by a white light interferometer. (**a**) The machined surface of diamond grinding tools. (**b**) The machined surface of micro-grinding tools.

To explain the cause of the above phenomenon from a microscopic perspective, a scanning electron microscope picture of the abrasive was taken, as shown in Figure 16. The powder crushing that occurs during the abrasive grinding process causes the bonds of the crystals on the surface of the powder to break. Due to the formation of unsaturated atomic valence states, chemical reactions occur between two solids or the solid and the surrounding gases. The factors affecting the degree of solid–solid phase chemical reaction mainly include (1) the crystal lattice distortion or defect formation of solid under the action of mechanical force. (2) Through mechanical crushing into a fine powder, the solid surface energy is changed, and the specific surface area is increased by producing a new solid surface to improve the degree of the chemical reaction. (3) Under applied force, some atomic groups will be generated on the newly formed surface of the solid due to structural fragmentation, thereby improving the degree of the chemical reaction. The role of calcium oxide is to act as a curing agent to promote resin curing, and it has high bonding strength and heat resistance; adding an appropriate amount of calcium oxide can better bond abrasives and additives together, thereby facilitating the solid–solid phase chemical reaction of the surface convex of the silicon wafer. The addition of zinc sulfate to the abrasive can make the adsorbent around the abrasive [21]; when the solid particles adsorb the medium, due to its increased volume, it is more likely to be broken when subjected to grinding collision, releasing a large amount of energy to increase the temperature of the contact zone, which is conducive to the solid–solid phase chemical reaction.

Figure 16. Scanning electron microscopy of the micro-grinding tool.

6. Conclusions and Outlook

In this paper, the development of micro-grinding tools and the research on their mechano-chemical grinding mechanism was carried out. The results showed that when the self-made micro-grinding tools grind single-crystal silicon, the chemical activity of the particles was first improved under the cumulative action of grinding force and grinding temperature. Then, the solid–solid phase chemical reaction occurred between the abrasives, additives, and the sharp points on the surface of the silicon wafer, and then the soft reactants generated were removed under the mechanical grinding of the micro-grinding tools to achieve high-quality and low-damage processing. This paper concluded as follows.

(1) The ε deformation coefficient of the contact geometry of the abrasive and silicon wafer was introduced. The grinding depth model was established by considering the geometric characteristics of the abrasive grain processing trajectory. Based on the established grinding depth model, the contact area grinding force model of single-crystal silicon grinding by the micro-grinding tools was established. The model showed that changes in the characteristics of the abrasive itself, including the abrasive diameter, elastic modulus, abrasive volume ratio, and other factors, would affect the grinding force. At the same time, changes in grinding parameters such as abrasive speed and cutting depth would also affect the change in grinding force;

(2) Self-made mechano-chemical micro-grinding tools could process single-crystal silicon into a very smooth mirror effect, and the surface roughness reached Ra1.332 nm. And the surface quality was close to that of the silicon wafer after chemical mechanical polishing (CMP) processing, and the surface was free of scratches, crushing pits, and other defects. The surface roughness of the silicon wafer after the diamond grinding tool processing was Ra96.363 nm, and there were obvious scratches on the surface and defects such as crushing. The processing effect of self-made mechano-chemical micro-grinding tools is much better than that of diamond grinding tools;

(3) In the process of grinding mechano-chemical micro-grinding tools, the instantaneous temperature of the surface of the silicon wafer could reach about 150 °C, which met the

temperature threshold conditions for solid–solid phase chemical reactions between cerium oxide and additives and single-crystal silicon. A soft compound was formed on the surface of the silicon wafer through a chemical reaction between silicon and cerium oxide abrasives and was removed by mechanical wear in the subsequent process, and ultra-low damage processing of single-crystal silicon was realized under the synergy of machinery and chemistry.

Author Contributions: Conceptualization, X.S. and Y.R.; methodology, X.S.; validation, K.Z.; formal analysis, F.K.; investigation, J.Z.; resources, W.L.; data curation, K.Z.; writing—original draft preparation, F.K.; writing—review and editing, X.S.; visualization, F.K.; supervision, W.L.; project administration, X.S. and Y.R. All authors have read and agreed to the published version of the manuscript.

Funding: The authors would like to appreciate the Special Sub-task of Strategic Leading Science and Technology of the Chinese Academy of Sciences (XDA25020317-05), Excellent Youth Project of Educational Committee of Hunan Province (2022JJ10010), Key Research and Development Program of Hunan Province (2022WK2003), the Natural Science Foundation of Hunan Province (2020JJ4193, 2021JJ40064) and the Natural Science Foundation of Changsha City (kq2014048).

Institutional Review Board Statement: Not applicable.

Informed Consent Statement: Not applicable.

Data Availability Statement: Not applicable.

Conflicts of Interest: The authors declare no conflict of interest.

References

1. Uhlmann, E.; Mullany, B.; Biermann, D.; Rajurkar, K.; Hausotte, T.; Brinksmeier, E. Process chains for high-precision components with micro-scale features. *CIRP Ann.* **2016**, *65*, 549–572. [CrossRef]
2. Chae, J.; Park, S.S.; Freiheit, T. Investigation of micro-cutting operations. *Int. J. Mach. Tools Manuf.* **2006**, *46*, 313–332. [CrossRef]
3. Dornfeld, D.; Min, S.; Takeuchi, Y. Recent Advances in Mechanical Micromachining. *CIRP Ann.* **2006**, *55*, 745–768. [CrossRef]
4. Robinson, G.; Jackson, M. A review of micro and nanomachining from a materials perspective. *J. Mater. Process. Technol.* **2005**, *167*, 316–337. [CrossRef]
5. Aurich, J.C.; Carrella, M.; Walk, M. Micro grinding with ultra small micro pencil grinding tools using an integrated machine tool. *CIRP Ann.* **2015**, *64*, 325–328. [CrossRef]
6. Wong, Y.S.; Rahman, M.; Asma, P.; Wong, Y.S. A study on microgrinding of brittle and difficult-to-cut glasses using on-machine fabricated poly crystalline diamond (PCD) tool. *J. Mater. Process. Technol.* **2012**, *212*, 580–593.
7. Haberland, R.; Schueler, G.M.; Engmann, J.; Haberland, R. Micro grinding tool for manufacture of complex structures in brittle materials. *CIRP Ann.* **2009**, *58*, 311314.
8. Zhou, L.B.; Kawai, S.; Honda, M. Research on mechano-chemical grinding (MCG) of Si wafer: 1st report: Development of MCG wheel. *Jpn. Soc. Precis. Eng.* **2002**, *68*, 1559–1663. [CrossRef]
9. Dai, H.Z.; Jiao, Z.H.; Wang, B. Mechano-chemical grinding for k9 optical glass. *Adv. Mater. Res.* **2014**, *1002*, 57–60. [CrossRef]
10. Huang, H.; Wang, B.L.; Wang, Y.; Zou, J.; Zhou, L. Characteristics of silicon substrates fabricated using nanogrinding and mechano-chemical grinding. *Mater. Sci. Eng. A* **2008**, *479*, 373–379. [CrossRef]
11. Zhou, L.B.; Shimizu, J.; Eda, H. A novel fixed abrasive process: Mechano-chemical grinding technology. *Int. J. Manuf. Technol. Manag.* **2005**, *7*, 441–454. [CrossRef]
12. Zhou, L.B.; Shimizu, J.; Eda, H.; Shimizu, J.; Eda, H.; Yakita, K. Research on mechano-chemical grinding (MCG) of Si wafer: 2nd report: Development of MCG wheel. *Jpn. Soc. Precis. Eng.* **2005**, *71*, 466–470.
13. Zhou, L.; Eda, H.; Shimizu, J.; Kamiya, S.; Iwase, H.; Kimura, S.; Sato, H. Defect-free fabrication for single crystal silicon substrate by mechano-chemical grinding. *CIRP Ann.-Manuf. Technol.* **2006**, *55*, 313–316. [CrossRef]
14. Wu, K.; Zhou, L.B.; Shimizu, J.; Onuki, T.; Yamamoto, T.; Ojima, H. Study on the potential of mechano-chemical grinding (MCG) process of sapphire wafer. *Int. J. Adv. Manuf. Technol.* **2017**, *91*, 1539–1546. [CrossRef]
15. Shimizu, J.; Tian, Y.B.; Zhou, L.B.; Tashiro, Y.; Kang, R.K. Elimination of surface scratch/texture on the surface of single crystal si substrate in mechano-chemical grinding (MCG) process. *Appl. Surf. Sci. A J. Devoted Prop. Interfaces Relat. Synth. Behav. Mater.* **2009**, *255*, 4205–4211.
16. Kang, R.K.; Gao, S.; Jin, Z.J.; Guo, D.M. Study on Grinding Performance of Soft Abrasive Wheel for Silicon Wafer. *Key Eng. Mater.* **2009**, *416*, 529–534. [CrossRef]
17. Dong, Z.G.; Gao, S.; Zhou, P.; Kang, R.K.; Guo, D.M. Grinding performance evaluation of the developed mechano-chemical grinding (MCG) tools for sapphire substrate. *Adv. Mater. Res.* **2012**, *565*, 105–110. [CrossRef]

18. Zhou, L.; Shiina, T.; Qiu, Z.; Shimizu, J.; Yamamoto, T.; Tashiro, T. Research on mechano-chemical grinding of large size quartz glass substrate. *Precis. Eng.* **2009**, *33*, 499–504. [CrossRef]
19. Sharp, K.W.; Scattergood, R.O.; Miller, M.H. Analysis of the grain depth-of-cut in plunge grinding. *Precis. Eng.* **2000**, *24*, 220–230. [CrossRef]
20. Wang, D.; Ge, P.; Bi, W.; Jiang, J. Grain trajectory and grain workpiece contact analyses for modeling of grinding force and energy partition. *Int. J. Adv. Manuf. Technol.* **2014**, *70*, 2111–2123. [CrossRef]
21. Younis, M.; Sadek, M.M.; El-Wardani, T. A New Approach to Development of a Grinding Force Model. *J. Eng. Ind.* **1987**, *109*, 306–313. [CrossRef]